www.rericjournal.ait.ac.th

Experiment on the Vibration Response of Horizontal Axis Wind Turbine Tower under Dynamic Vehicle Loading

X.F. Liu*, Q.Y. Li[@], W.M. Wu[#], W.J. Liu[$], S.C. Zhang[&], and Y.Q. Pan[#]

ARTICLE INFO

Article history:
Received 28 August 2023
Received in revised form
02 January 2024
Accepted 12 January 2024

Keywords:
Horizontal axis wind turbine
Impeller tower
Structural vibration
Vehicle test
Vibration frequency

ABSTRACT

Under unstable wind loads, the wind turbine tower, as a supporting component of the horizontal axis experiences inevitable vibration. To explore the vibration characteristics of the tower, a vehicle test platform is established to measure the vibration acceleration component signals at different heights of a 300W small horizontal axis wind turbine tower. The results show that specific vehicle vibration test equipment can accurately test the vibration characteristics and laws of small wind turbine towers. The main vibration form of the tower is low frequency, with noticeable axial vibration at the top and lateral vibration in the middle of the tower due to aerodynamic load from natural wind. These findings can be used as a valuable reference for the safety and reliability design of the whole machine and the low-frequency vibration status monitoring of wind turbines.

1. INTRODUCTION

The tower of a wind turbine plays a crucial role in supporting the nacelle and wind alternator at the required height. Throughout the lifespan of the turbine, the tower is subjected to various loads including the wind alternator, engine room and gravity, and dynamic forces from different wind conditions (normal wind conditions, and extreme wind conditions), and bears fatigue loads and limit loads that change in size and direction at any time. During operation, excessive tower vibrations can lead to shutdowns, affecting the safety and stability of the wind turbine. As wind turbines grow towards large-scale megawatts, the flexibility of the towers become more and more significant. Vibrations of the tower caused by moving loads such as wind, waves, and earthquakes are becoming more and more obvious. It is easy to cause meshing failure of gears, transmission shafts, generators and other components in the nacelle, as well as loosen and shared connecting bolts at the bottom of the tower. In severe cases, it may cause damage to the entire unit and other malignant disasters [1]. To this end, vibration stability has become the primary concern and problem of the unit in design. Ensuring vibration stability is a major concern in the design process of wind turbines [2]. Through measurement and analysis of tower vibrations, the vibration amount and frequency composition of the tower during the actual working process can be understood and the design can be verified.

Due to the large sizes of wind turbine towers, experimental testing is difficult. There are few experimental studies on the vibration characteristics of towers under natural wind. Their vibration frequency and mode characteristics are mainly obtained by finite element method using commercial software simulation. Wang [3] used the ANSYS finite element analysis method and the block lanczos method to calculate the frequency and mode of vibration of a 1.5 MW wind turbine tower under extreme wind loads. Lei *et al.* [4] used the ANSYS dynamic time history analysis method to verify the effectiveness of a pre-stressed tuned mass damper PS-TMD in reducing the dynamic response of the tower due to fundamental frequency resonance. Xiang [5] used GH Bladed software to analyze the mode of an 8MW offshore wind turbine tower and identify the main sources and frequency resonance zones of tower vibration using a Campbell diagram. Based on the characteristics of multi-frequency vibration and time-varying coupling of large wind turbine towers, Yang *et al.* [6] proposed a knowledge-driven parallel adaptive notch filter to track tower vibration at multiple frequencies and eliminate the influence of vibration components at each frequency. They also used FAST and Matlab to simulate the vibration of the tower of the NERL 5 MW wind turbine to verify the effectiveness of the proposed method. In terms of physical models, Gu *et al.* [7] used the Multi Body System Transfer Matrix

*Yinchuan University of Science and Technology, Yinchuan, 750001, China.

[@]Inner Mongolia University of Technology, Hohhot, 010080, China.

[#]Chongqing University of Science and Technology, Chongqing, 401331, China.

[$]Chongqing Technology and Business Institute, Chongqing, 400052, China.

[&]Inner Mongolia Three Gorges Mengneng Energy Co., Ltd., Hohhot, 010090, China.

[1]Corresponding author:
Email. wu202167@163.com

Method (MSTMM) to simplify the physical model and established a multi-body dynamic model of the tower system. The dynamic response of the flexible tower was calculated by coupling the modal vibration mode with the two-degree-of-freedom wake oscillator model. Xiao [8] simplified the structure of a 1.5MW wind turbine tower into a variable section cantilever beam to establish a finite element model. The static strength and stiffness of the tower were checked under the rated wind speed, cut-out wind speed, and maximum wind speed respectively. The ole integral method was used to program the displacement at the top of the tower to analyze its free mode. They found that the mass at the top of the tower had a great influence on its natural frequency. Li *et al.* [9] established an overall model of the tower-blade coupling structure of a 5MW wind turbine, proposing its dynamic equations. Based on the natural frequency and mode shape parameters of different structures, the influence of the coupling of wind turbine tower-blade on the vibration of blade structure was analyzed. The main modal frequency of the tower-blade coupling structure was 55%-84% smaller than that of a single blade. The coupling structure and the first four mode shapes of a single blade had the same characteristics. Regarding the unique wall thickness segmented structure of wind turbine towers, Guan and Tian [10] derived the mode shape function of the tower based on the approximate differential equation of the deflection curve. Combined with the Rayleigh method, the approximate solution of the first-order natural frequency of the tower was derived. The empirical formula for the first-order natural frequency estimation of a 2 MW tower was fitted, aiming to provide a certain theoretical basis for the structural design of wind turbine towers. Deng *et al.* [11] proposed a calculation model for the vibration and stress state of a wind turbine tower based on the modal superposition method. In response to the inherent defects of vibration sensors in ultra-low frequency absolute vibration measurement and cannot accurately measure the natural frequency of wind turbine towers, Yu *et al.* [12] proposed to use strain gauge mode to measure the natural frequency of wind turbine towers. For units with low-frequency vibrations, Chen *et al.* [13] used the traditional dynamic method to analyze the modal state of blades, nacelles and tow**e**rs. The natural frequency of the tower was tested by using the modal testing equipment and compared it with the designed natural frequency, so as to determine its state during operation. Malliotakis *et al.* [14] highlighted the benefits of mounting structural systems in reducing tower vibration loads, thereby improving their structural reliability and resilience to extreme events. They found that the random characteristics of typical tower loads remained a key issue for the design and performance of state-of-the-art vibration control methods. Considering the flexibility of the tower and foundation, taking the tower as Diken and Asiri [15] regarded the tower as a Rayleigh beam with a flexible foundation, and derived the ten-degree-of-freedom dynamic equation using the Lagrange equation to study the coupling vibration of onshore horizontal axis wind turbines. They found that the inertia of the rotor-bearing system reduced the natural frequencies of the front, rear, left and right of the tower by 35%. Pollini *et al.* [16] proposed a constraint analysis based on the Lagrange multiplier and relative cost index. They found that for rigid-rigid and soft-rigid designs, the 3P tower frequency constraint had the greatest impact on cost. This design was found to be 11% cheaper than the soft-rigid design.

In terms of experimental testing, Yan *et al.* [17] simulated the dynamic changing direction of wind through a dynamic rotating platform, and studied the stress change of dynamic wind at the top and bottom of the tower and its influence on the stress of the tower. Wu *et al.* [18] conducted modal analysis and operational modal tests on a horizontal axis fan tower using a dynamic signal acquisition and analysis system. The natural frequencies and vibration modes of the tower under static and vibration conditions were obtained. Chen *et al.* [19] used a vibration test system to test and analyze the axial and lateral vibration signals at different height measurement points of small horizontal axis wind turbine towers. The results indicated that when the tower was non-resonant, its lateral vibration amplitude was greater than the axial vibration. When the fundamental frequency of the wind motor rotation approached the natural frequency of the first-order bending vibration of the tower, resonance occurs in the tower, and the axial vibration amplitude of the tower was greater than the lateral vibration.

Most research on tower vibration mainly focus on simulation. However, there are few studies on tower vibration test, especially on tower vibration of large units. This study aim to address this gap by using the Donghua DH5902N robust vibration test equipment as the core of a dynamic vibration acceleration acquisition system. The system was used to conduct on-board tests on small wind turbine towers, taking into account the relationship between the moving vehicle and the incoming flow. This approach allows for vibration testing of large wind turbine towers in real environments, which is currently difficult to achieve. In addition, it provides a means to conduct vibration tests on small wind turbine towers that do not have wind tunnel conditions. The vibration acceleration test on a 300W small wind turbine tower under rotating excitation is carried out to explore the vibration characteristics of small wind turbine towers.

2. VIBRATION PRINCIPLE

The tower of a wind turbine is subjected to various forces such as the gravity of the wind motor and nacelle, as well as the comprehensive force system of the wind motor on the wind resistance and foundation damping. Due to the coupling structure of the wind motor, nacelle, tower and foundation, the stress at the top of the tower is high, and the rotational inertia at the bottom of the tower is also high. When the tower is subjected to the combined forces, its deformation and vibration are crucial for the stable operation of the wind turbine. Therefore, analyzing the tower mode shape and natural

frequency of wind turbines is essential to take control measures.

2.1 Tower Natural Frequency

In practice, the mass of a tower accounts for about half of the total mass of the wind turbine, which has a strong correlation with the height. The natural frequency is an important factor that determines the properties of the tower and affects the vibration. Therefore, when studying tower vibration and natural frequency, the tower quality cannot be ignored. The natural frequencies of the tower are as follows:

$$f = \frac{1}{2\pi}\sqrt{\frac{3EI}{(m_1 + 0.236 \cdot m_s)L^3}} \quad (1)$$

where, f is the natural frequency of the tower; E is the elastic modulus of the tower material; I is the moment of inertia of the tower section; m_1 is the equivalent block mass of the wind alternator and nacelle; L is the height from the center of the hub to the ground, and m_s is the mass of the tower.

2.2 Tower Vibration Mode

The vibration of any object is related to vibration energy, and the vibration of wind turbines is mainly provided by wind load. When the load is applied to components such as wind motor and tower nacelle, excitation forces such as wind motor thrust, blade swing and oscillation, and tower surface thrust are generated. When the flexible tower damping is not considered, the relationship between excitation force and tower vibration is as follows [18]-[19]:

$$m_s \frac{d^2x}{dt^2} + k_s x = F_0 \sin \omega t \quad (2)$$

where, m_s and k_s are the mass and stiffness of the tower, respectively; x(t) is the vibration displacement of the tower; F_0 is the external excitation force, and ω is the excitation angular frequency [19].

$$x = \frac{F_0 \sin \omega t}{k_s\left(1 - \left(\frac{\omega}{\omega_0}\right)^2\right)} \quad (3)$$

where, ω_0 is the natural angular frequency of the tower.

When the angle frequency ω of the excitation force and the natural angular frequency ω_0 of the tower is equal, the vibration displacement of the tower is infinitely large, which is called resonance of wind turbines. The excitation force is directly proportional to the tower vibration displacement. When the frequency of the excitation force remains constant, the tower vibration displacement increases as the excitation force increases. In this way, the overlap of the excitation force frequency and the natural frequency of the tower is the key factor causing the resonance of the tower. The influence of excitation force amplitude cannot be ignored in the same way. The vehicle vibration test is conducted here on the rigid tower of a 300 W small wind turbine.

This experimental study aims to understand the vibration characteristics of a rigid tower in a small wind turbine when exposed to natural wind. A 300W small wind turbine was used for this study. Instead of applying an artificial force, the natural wind at varying speeds was allowed to act on the tower during the on-board vibration test. To accurately measure and analyze the vibration acceleration, acceleration sensors were employed at different heights of the tower, avoiding any vibration errors introduced by a more complex measurement system.

3. TEST EQUIPMENT AND TESTING SCHEME

3.1 Test Equipment

The tested parameters of a 300 W small wind turbine are shown in Table 1. The data acquisition equipment adopts Donghua DH5902N rugged data acquisition and analysis system, with a dimension of 290×150×206 *mm* and a weight of 8.2 *kg*. The system is designed for data acquisition in various harsh environments, such as vehicle-mounted, airborne, and shipborne. The system described is equipped with an industrial-grade control computer and electronic hard disk. It is designed to complete testing and long-term monitoring work in extreme environments, such as strong vibration, high and low temperature, and high humidity. This system is suitable for signal acquisition in GB/T 6587-2012 Group III. harsh environment, with an impact resistance of $100g/(4\pm1)m_s$, a working temperature range of -20°C-+60°C, IP65 protection level. It can meet the demanding requirements of unsupervised and long-term uninterrupted data recording and can be used for vibration and performance testing in special testing scenarios such as vehicle-mounted, airborne, and shipborne. Its testing features are as follows:

(1) Frequency cycle range: 5Hz-55Hz-5Hz;
(2) Drive amplitude (peak): 0.19mm;
(3) Sweep rate: Less than or equal to 1 octave /min;
(4) Hold time at resonance point: 20min;
(5) Vibration direction: *x*, *y*, and *z*.

The test equipment is shown in Figure 1.

Fig. 1. DH5902N data acquisition system.

Table 1. Main design parameters of the test wind turbine.

Items	Parameters	Items	Parameters
Wind turbine	300 W	Tail rod quality	0.25 *kg*
Blade number	3	Tail fin quality	0.65 *kg*
Tower height	1.9 *m*	Diameter of the wind impeller	1.44 *m*
Airfoil (SD2030)	8.56% (f)	Rated wind speed	10 *m/s*
Eccentricity	0.050 *m*	Caster angle (adjustable)	8°
Tail rod length	0.56 *m*	Roll angle (adjustable)	12°
U-shaped unit quality	1.1 *kg*	Net weight of the wind turbine	11.5 *kg*

3.2 Test Scheme

3.2.1 Testing principles

The test wind turbine is a 300 W distributed small unit, and the specific design parameters are shown in Table 1. The tower to be measured has a height of 1.4 meters and a mass of 6.0 kilograms. The vehicle test platform is shown in Figure 2(a). The vibration acceleration sensors were respectively arranged at the bottom, middle and top of the tower. A 300 W small wind turbine was firmly fixed to the bottom of the pickup truck with DH5902N data acquisition module. The test section is a newly built straight asphalt road with a total length of about 10 *km*. The road surface is smooth and barrier-free, ensuring that pickup trucks equipped with wind turbines and a complete set of testing equipment can run smoothly at different speeds. 8 channels of the block were connected to collect vibration acceleration data at different heights of the tower. At the same time, real-time power measurement was carried out in conjunction with the power testing system of the small wind turbine. The special dynamic characteristics of each monitoring position of the tower were measured when the output power of the standby group was stable.

3.2.2 Coordinate system of the tower and layout of measurement points

As shown in Figure 2(b), a fixed coordinate system O-xyz at the bottom of the tower is established. The origin O is located in the geometric center of the base surface of the tower. The flow direction is positive z; the vertical ground is positive x, and the vertical xz plane is positive y.

To obtain the actual vibration acceleration parameters at different heights of the tower, three measurement points are arranged from bottom to top along the height of the tower. Sensors **1#**, **3#**, and **2#** are pasted in the downwind direction of each measurement point to measure the vibration acceleration signals at the bottom, middle, and top of the tower. Considering the influence of the foundation damping at the bottom of the tower and the deformation of the large deflection at the top of the tower, a 3D acceleration sensor is arranged at the bottom and top of the tower, respectively. Due to the fact that the tower only bears the incoming wind load, only one two-dimensional acceleration sensor is installed in the middle of the tower.

Three sensors are connected to the DH5902N data acquisition system. AI101-AI10 channels of the acquisition instrument are connected to sensor **1#**, to measure the vibration acceleration signals in the x, y and z directions at the bottom of the tower; AI104-AI106 channels are connected to sensor **2#**, to measure the vibration acceleration signals in the x, y and z directions at the top of the tower; AI107-AI108 channels are connected with sensor **3#**, to measure the vibration acceleration signal in the x and y directions in the middle of the tower. The test process and sensor placement are shown in Figure 2.

As shown in Figure 2(b), a fixed coordinate system O-xyz at the bottom of the tower is established.

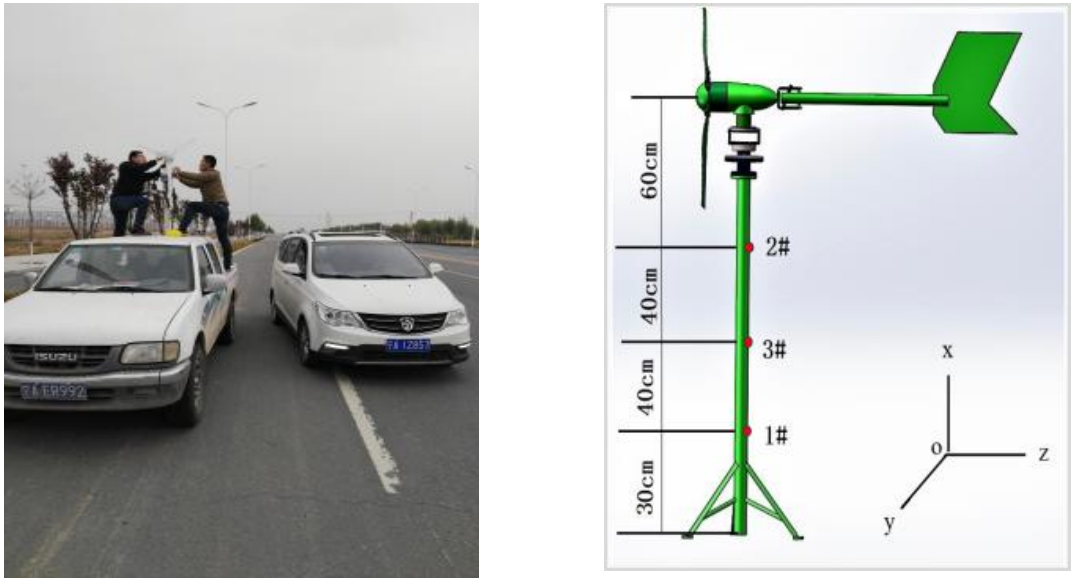

(a) Vehicle test site (b) Measurement point location

Fig. 2. Test site and sensor layout.

3.2.3 Specific experiment procedures

The specific arrangement of the experiment is generally divided into the preparation phase and the experimental phase, as shown in Figure 3. The preparation stage involves installing the on-board experimental wind turbine and gravity speed regulating device, adjusting the balance weight of the wind turbine tail rudder and the length of the wind turbine tail rod. At the same time, the wind turbine vibration measuring equipment, impeller power and angular velocity measuring equipment and wind speed measuring equipment are installed. In addition, the experimental road conditions, environmental weather and so on should be investigated.

This experimental phase involves conducting experimental tests using the same tail-rudder shape and weight but varying wind speeds based on the same tail-rudder shape and weight. The test is repeated 10 times for each wind speed, and the average data value in this condition can be calculated after removing the invalid data. Finally, the experimental wind speed, impeller angular speed, yaw angular speed, vibration signal and other relevant information are sorted out and recorded.

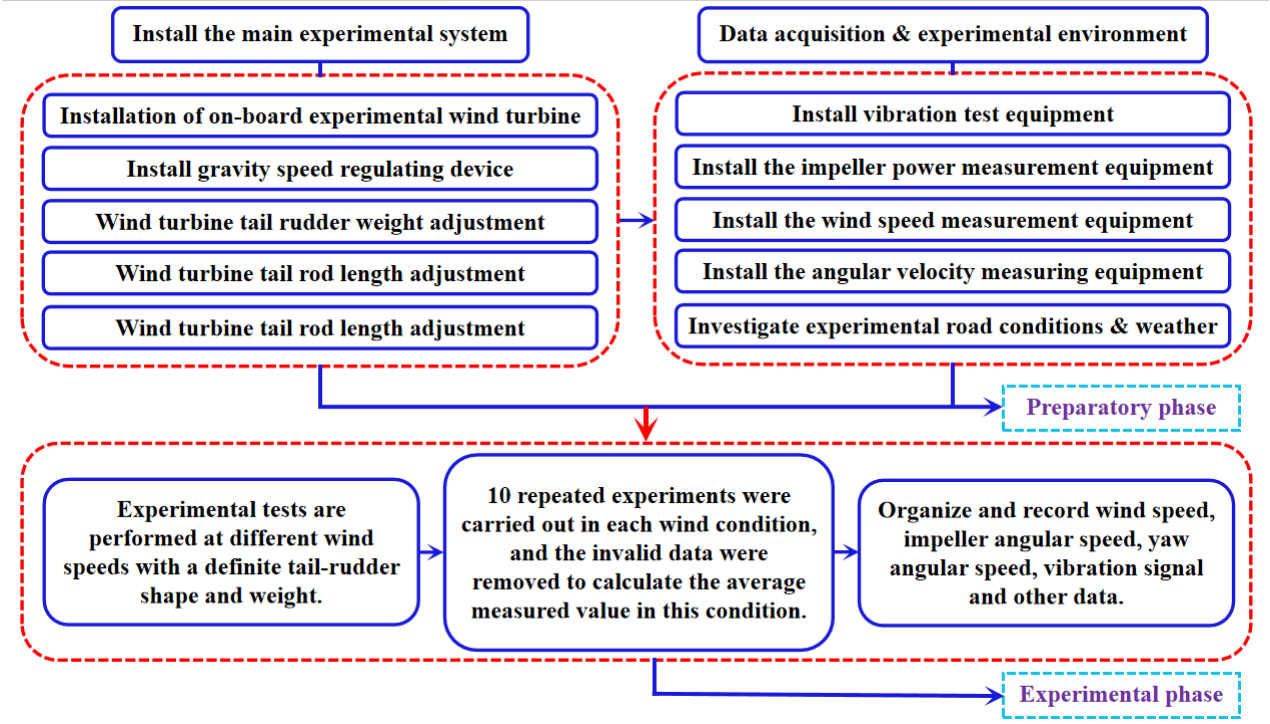

Fig. 3. The detailed flow chart of vibration experiment of vehicle-mounted wind turbine.

4. ANALYSIS OF TEST RESULTS

4.1 Analysis of Power Characteristics of Wind Turbines

The power test and tower vibration test are conducted simultaneously, with a total of three sets of tests with the following three working conditions:

(1) Condition 1: The table speed is 50km/h; the average wind speed is about 12m/s, and the measurement time is 28s;

(2) Condition 2: The table speed is 60km/h; the average wind speed is about 14m/s, and the measurement time is 32s;

(3) Condition 3: The table speed is 70km/h; the average wind speed is about 16m/s, and the measurement time is 43s.

The actual wind speed, yaw angle, rotor speed, and output power of the wind turbine under the three conditions are shown in Figure 4.

According to Figure 4, it can be seen that under the three working conditions, the wind turbine operates smoothly and stably with the wind speeds of 12 *m/s*, 14 *m/s*, and 16 *m/s*, wind motor speeds of 860 *r/min*, 960 *r/min*, and 1020 *r/min*, yaw angles of 50 *deg*, 60 *deg*, and 63 *deg*, and output powers of 152 W, 170 W, and 175 W, respectively. This provides a necessary condition for the accuracy of tower vibration tests on this basis.

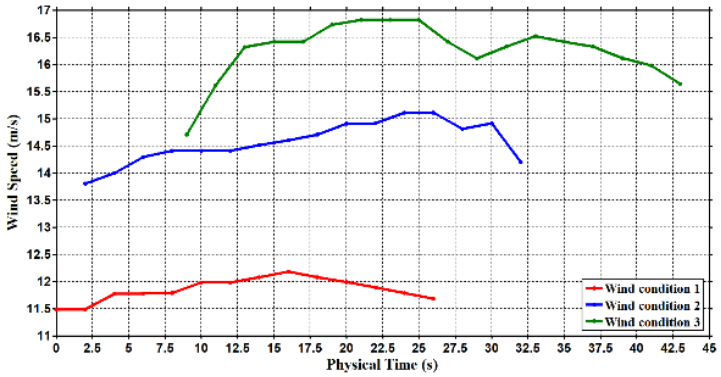

(a) wind speed variation

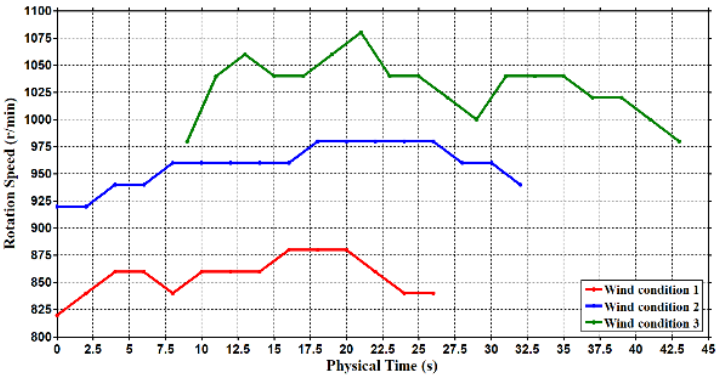

(b) rotational speed variation

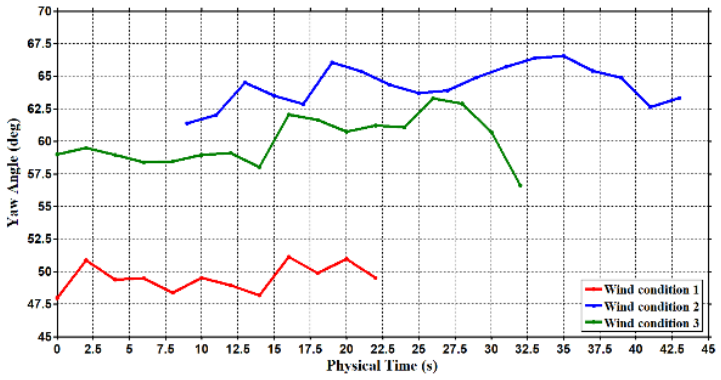

(c) yaw angle variation

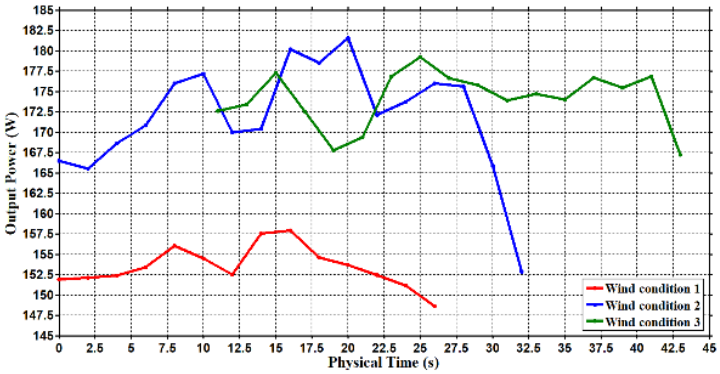

(d) output power variation

Fig. 4. Actual operation parameters of the wind turbine under the three working conditions.

4.2 Analysis of Tower Vibration Characteristics

4.2.1 Time-domain analysis of vibration acceleration

Considering that the wind turbine can operate stably under the three conditions, the vibration acceleration components at different heights of the tower are further measured. The time-domain distribution of the measured vibration acceleration is shown in Figures 5 to 7, respectively.

At the same time, this study have to know that the red, blue, and green correspond to the acceleration components in the x, y, and z directions, respectively. Figures 5 to 7 show that the vehicle tests can accurately capture the real-time vibration acceleration component time-domain spectra of the wind turbine tower at various heights under the three conditions.

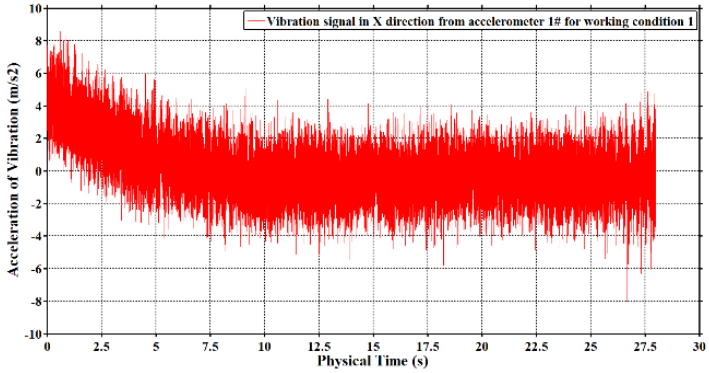

(a)

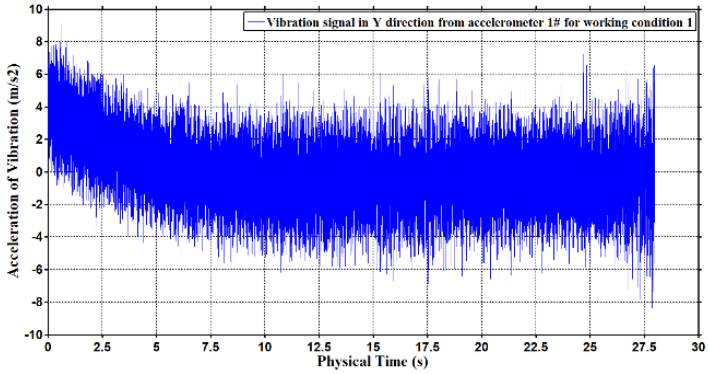

(b)

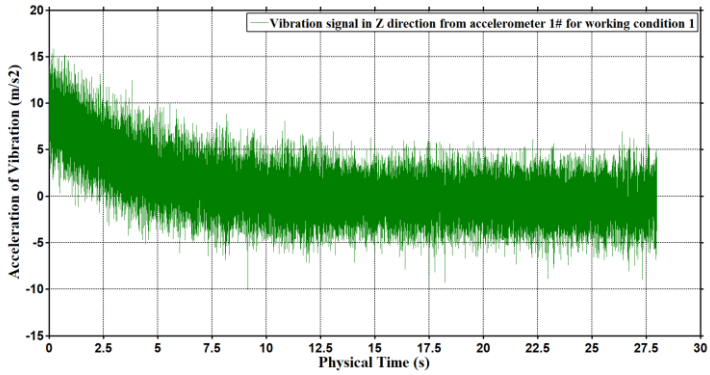
Vibration signal in Z direction from accelerometer 1# for working condition 1
Acceleration of Vibration (m/s2)
Physical Time (s)

(c)

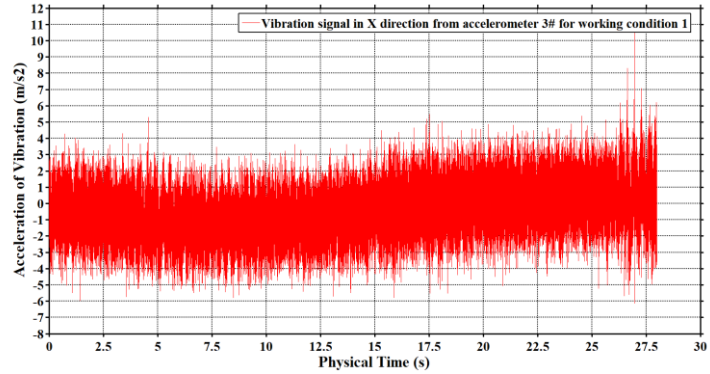
Vibration signal in X direction from accelerometer 3# for working condition 1
Acceleration of Vibration (m/s2)
Physical Time (s)

(d)

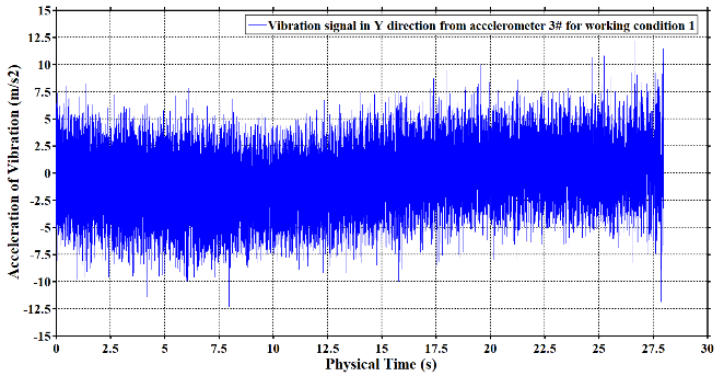
Vibration signal in Y direction from accelerometer 3# for working condition 1
Acceleration of Vibration (m/s2)
Physical Time (s)

(e)

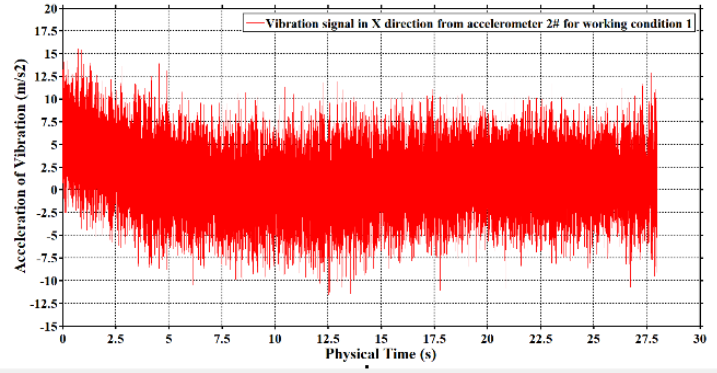
Vibration signal in X direction from accelerometer 2# for working condition 1
Acceleration of Vibration (m/s2)
Physical Time (s)

(f)

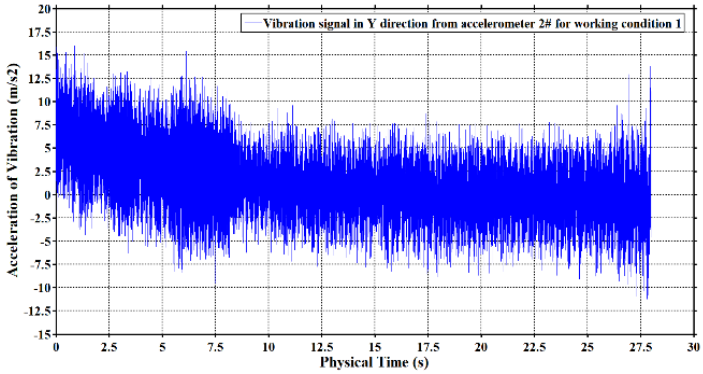

(g)

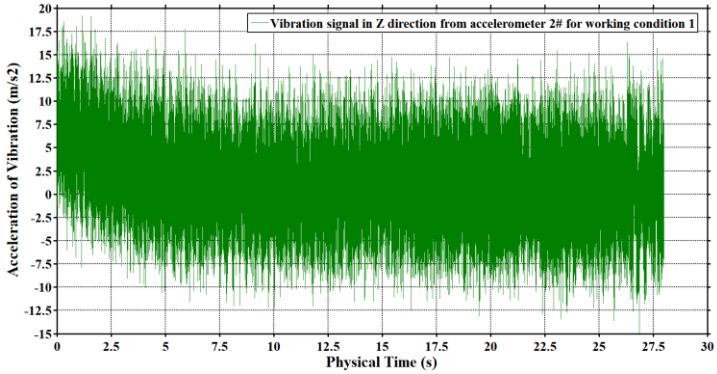

(h)

Fig. 5. Time-domain distribution of vibration acceleration components at different heights of the tower at Condition 1: (a) - (c): Acceleration components measured by Sensor 1# at the bottom of the tower; (d)-(e): Acceleration components measured by Sensor 3# in the middle of the tower; (f) -(h): Acceleration components measured by Sensor 2# at the top of the tower.

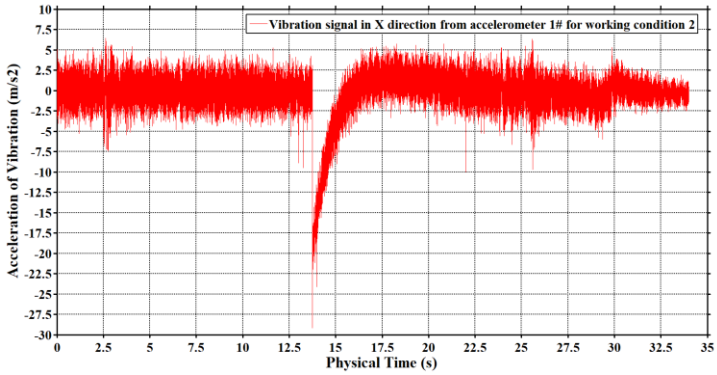

(a)

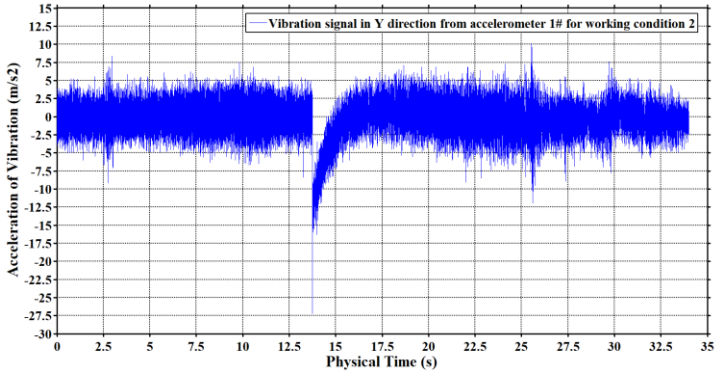

(b)

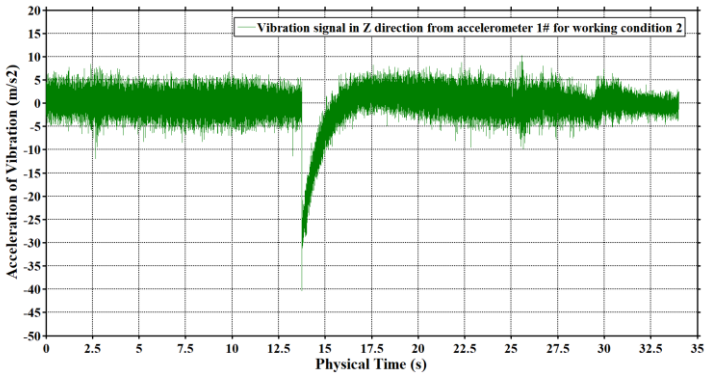
Vibration signal in Z direction from accelerometer 1# for working condition 2
Acceleration of Vibration (m/s2)
Physical Time (s)

(c)

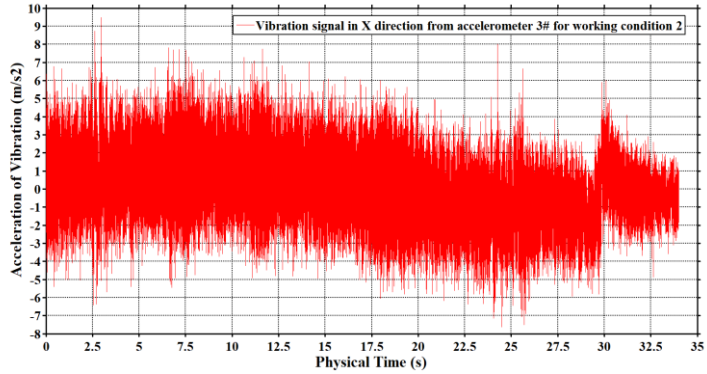
Vibration signal in X direction from accelerometer 3# for working condition 2
Acceleration of Vibration (m/s2)
Physical Time (s)

(d)

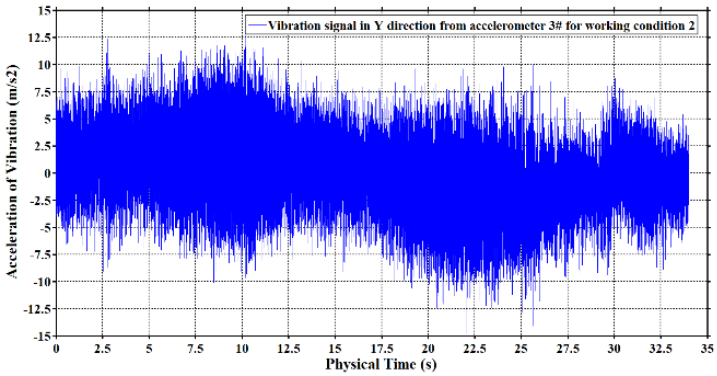
Vibration signal in Y direction from accelerometer 3# for working condition 2
Acceleration of Vibration (m/s2)
Physical Time (s)

(e)

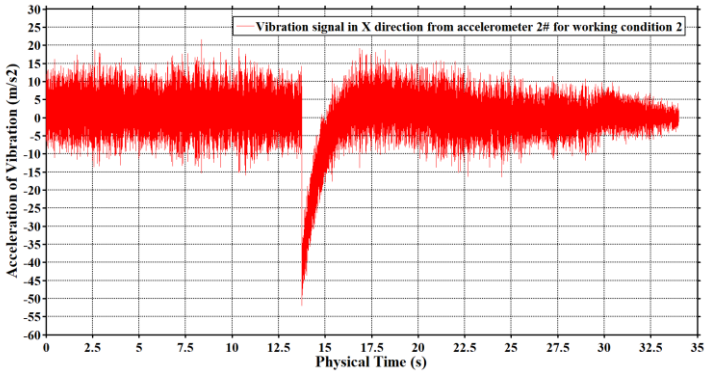
Vibration signal in X direction from accelerometer 2# for working condition 2
Acceleration of Vibration (m/s2)
Physical Time (s)

(f)

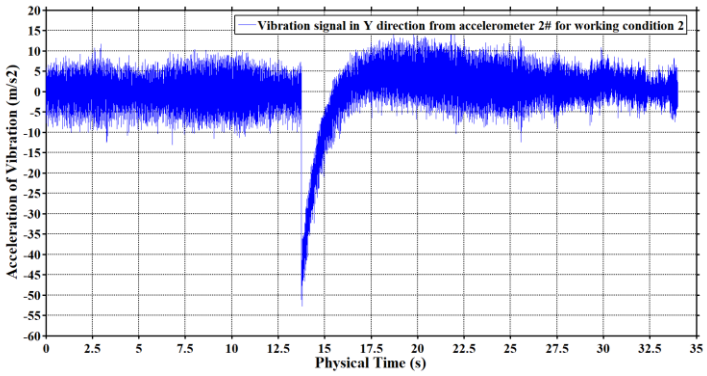

(g)

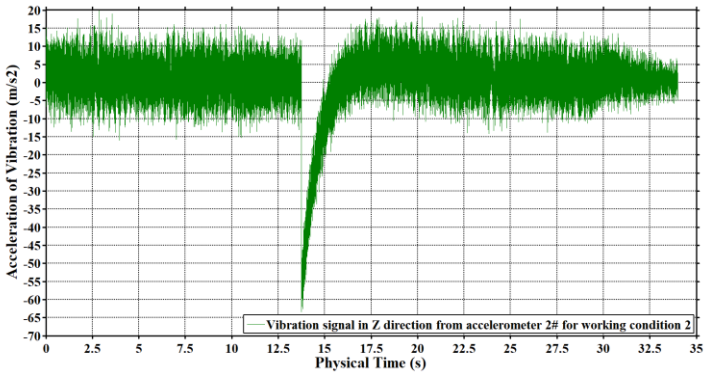

(h)

Fig. 6. Time-domain distribution of vibration acceleration components at different heights of the tower at Condition 2: (a)-(c); Acceleration components measured by Sensor 1# at the bottom of the tower; (d) - (e): Acceleration components measured by Sensor 3# in the middle of the tower; (f) - (h): Acceleration components measured by Sensor 2# at the top of the tower.

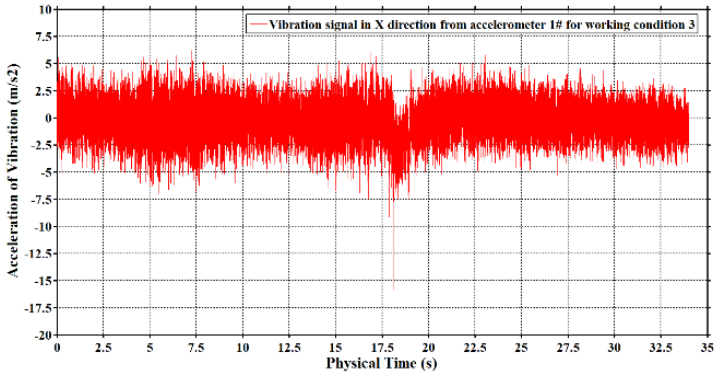

(a)

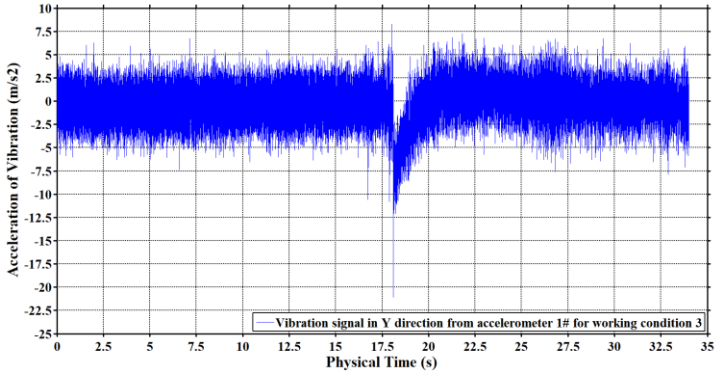

(b)

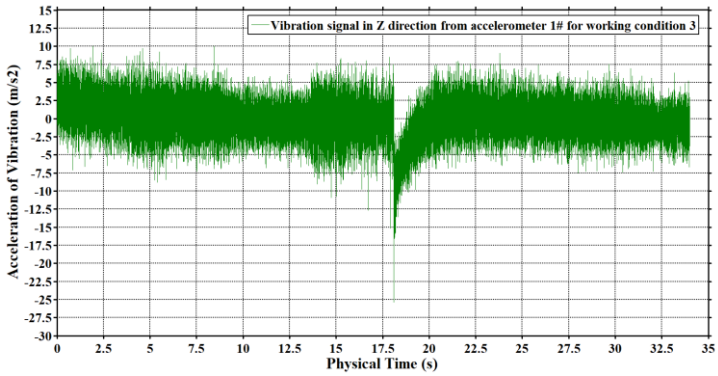
Vibration signal in Z direction from accelerometer 1# for working condition 3
Acceleration of Vibration (m/s2)
Physical Time (s)

(c)

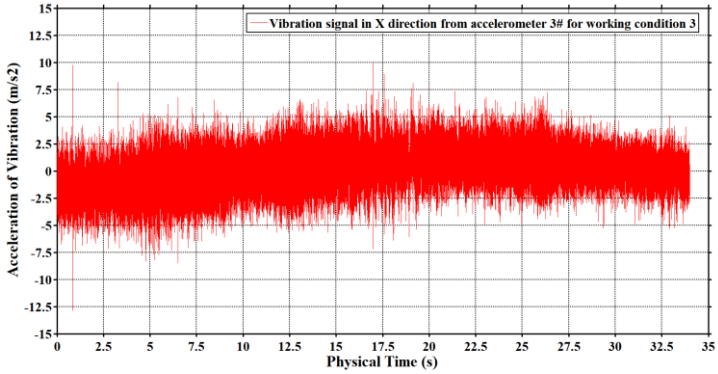
Vibration signal in X direction from accelerometer 3# for working condition 3
Acceleration of Vibration (m/s2)
Physical Time (s)

(d)

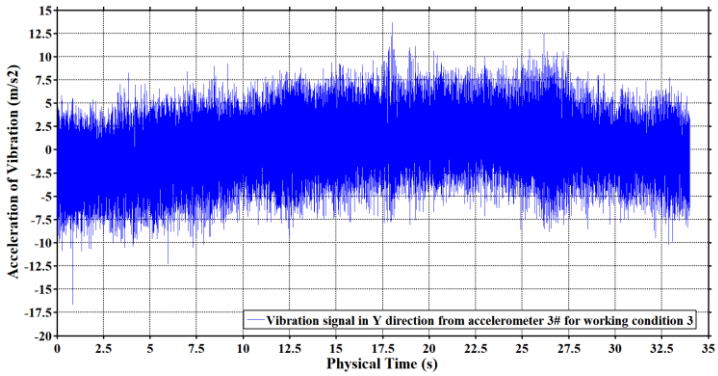
Vibration signal in Y direction from accelerometer 3# for working condition 3
Acceleration of Vibration (m/s2)
Physical Time (s)

(e)

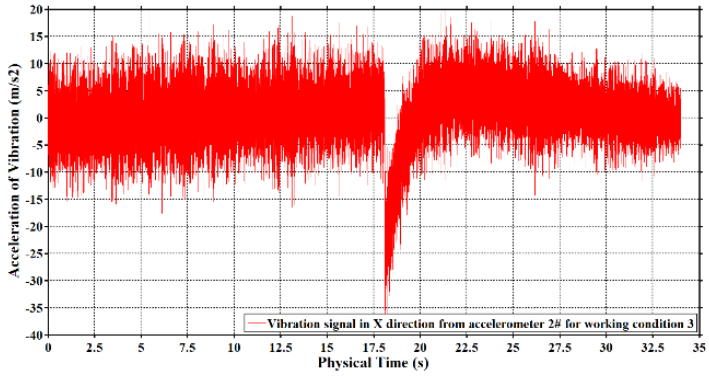
Vibration signal in X direction from accelerometer 2# for working condition 3
Acceleration of Vibration (m/s2)
Physical Time (s)

(f)

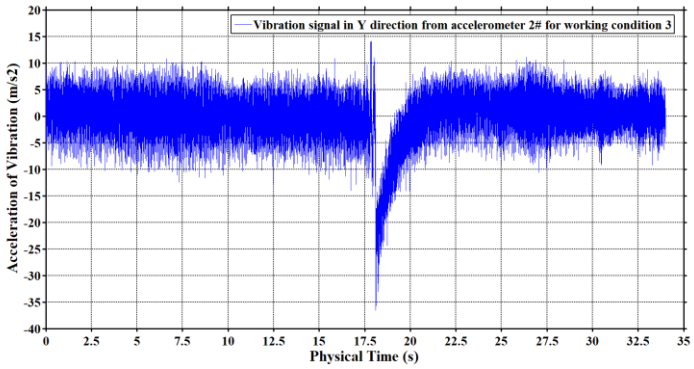

(g)

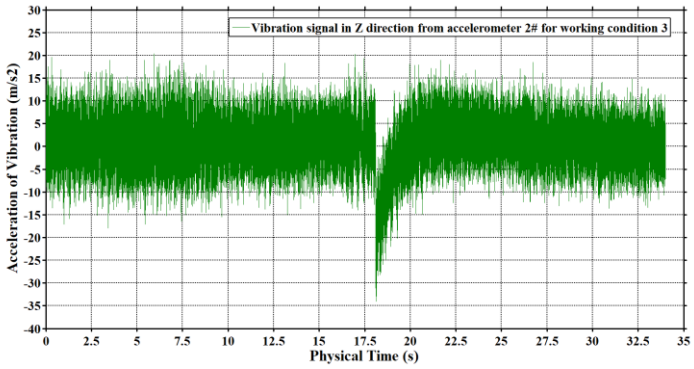

(h)

Fig. 7. Time-domain distribution of vibration acceleration components at different heights of the tower at Condition 3: (a) - (c): Acceleration components measured by Sensor 1# at the bottom of the tower; (d) - (e): Acceleration components measured by Sensor 3# in the middle of the tower; (f) - (h): Acceleration components measured by Sensor 2# at the top of the tower.

As shown in Figures 6 to 7, except for (d) and (e), there is a significant acceleration mutation in the time-domain of the vibration acceleration components, while (a)- (c) and (f) - (h) are near at t = 13.75 *s* and 18.75 *s*, respectively. There is no such mutation in Figure 5. This is mainly because the truck loading and testing the wind turbine had speed bumps on the road during the test. Comparing Figures 5 to 7, it can be found that this speed bump only has an effect on the vibration acceleration component at the bottom and top of the tower and has no effect in the middle of the tower. This may be because the tower is 1.7 *m* high and rigid. Sensor **3#** in the middle of the tower is 0.7 *m* away from the bottom of the tower and 1.0 *m* away from the center of the hub and is not obviously affected by the speed bump. Sensor 1# at the bottom and Sensor 2# at the top of the tower are more sensitive to the influence of the speed bump, and they are also affected by the base damping and aerodynamic load, respectively.

To quantify the vibration characteristics of the tower at different heights in vehicle testing, the time-domain spectrum range of the vibration acceleration component measured under the three working conditions is analyzed, as shown in Table 2.

Table 2. Time-domain spectrum range and width of vibration acceleration components at different heights of the tower.

Locations		Condition 1		Condition 2		Condition 3	
		Spectral range	Spectral width	Spectral range	Spectral width	Spectral width	Spectral width
1# (bottom)	*x*	-4~4	8	-5~5	10	-5~5	10
	y	-6~6	12	-5~5	10	-5~5	10
	z	-5~5	10	-5~5	10	-7.5~7.5	15
3# (middle)	*x*	-5~5	10	-6~6	12	-5~5	10
	y	-7.5~7.5	15	-10~10	20	-7.5~7.5	15
2# (top)	*x*	-7.5~10	17.5	-10~15	25	-15~15	30
	y	-7.5~7.5	15	-10~10	20	-10~10	20
	z	-10~12.5	22.5	-10~15	25	-15~15	30

Comparing the time-domain spectral width of the vibration acceleration component at different positions of the tower under three working conditions, it is found that:

From Condition 1 to Condition 3, as the wind speed increases, only the width of the time-domain spectrum of acceleration in the x, y, and z directions measured by Sensor 2# at the top of the tower gradually increases. Meanwhile, Sensor 1# at the bottom of the tower and Sensor 3# in the middle of the tower do not have this pattern, indicating that the vibration at the top of the tower is significant. This is because the tower top is greatly affected by the aerodynamic load, indicating that the vibration at the top of the tower is mainly caused by the aerodynamic load.

Under the same working conditions, that is, when the wind speed is invariable, the width of the time-domain spectrum of acceleration in the x, y and z directions measured by Sensor 1# at the bottom of the tower is the smallest. At the same time, from the bottom to the middle, and then to the top of the tower, the width of the time-domain spectrum of the acceleration component in all directions gradually increases. This is because fixed constraints are applied at the bottom of the tower, resulting in vibration damping, which is consistent with the law of the bending vibration mode of the tower.

At the same location, the time-domain spectral width of the y-direction acceleration of Sensor 1# at the bottom of the tower is only greater than that in the x direction under Condition 1, and the other two conditions are equal. In these three conditions, the time-domain spectral widths of the acceleration in the x direction of Sensor 3# in the middle of the tower are all smaller than in the y direction, and that of Sensor 3# at the top of the tower are all greater than in the y-direction. Meanwhile, the time-domain spectral width of the acceleration in the z direction is the largest. It indicates that as tower height and wind speed increase, the z direction vibration response at the top of the tower is the most obvious, while the vibration response in the x and y directions is related to the wind speed and height.

4.2.2 Frequency spectrum analysis of vibration acceleration

To further analyze the vibration characteristics of the tower from the perspective of vibration frequency, the Fourier transform on the measured time-domain signal is carried out. The frequency domain distribution of the vibration acceleration component at different positions of the tower under the three conditions is obtained, as shown in Figures 8 to 10.

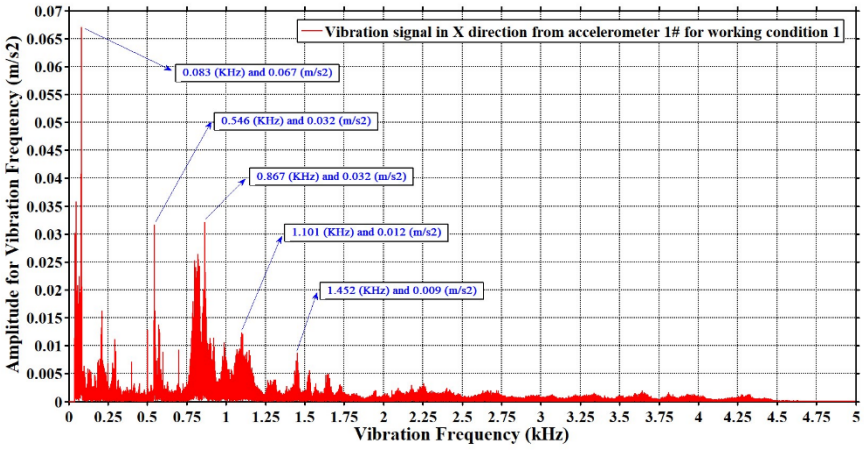

(a)

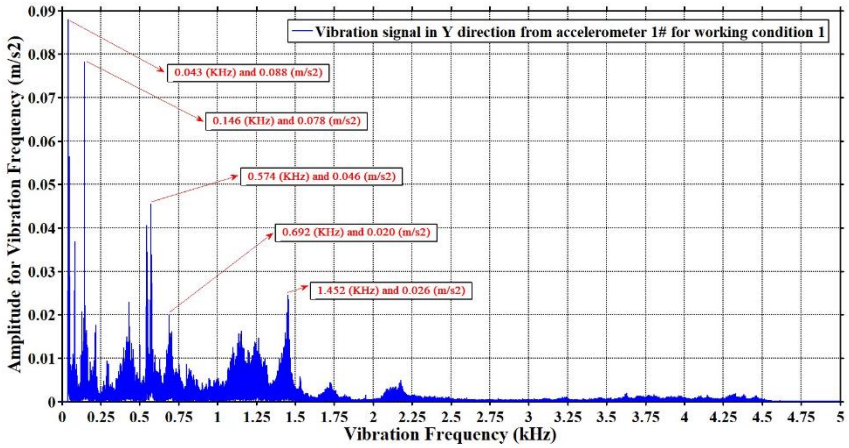

(b)

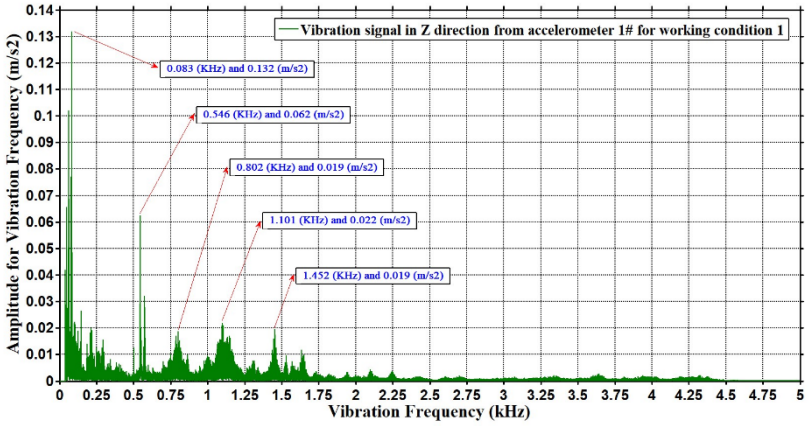
Vibration signal in Z direction from accelerometer 1# for working condition 1
0.083 (KHz) and 0.132 (m/s2)
0.546 (KHz) and 0.062 (m/s2)
0.802 (KHz) and 0.019 (m/s2)
1.101 (KHz) and 0.022 (m/s2)
1.452 (KHz) and 0.019 (m/s2)
Amplitude for Vibration Frequency (m/s2)
Vibration Frequency (kHz)

(c)

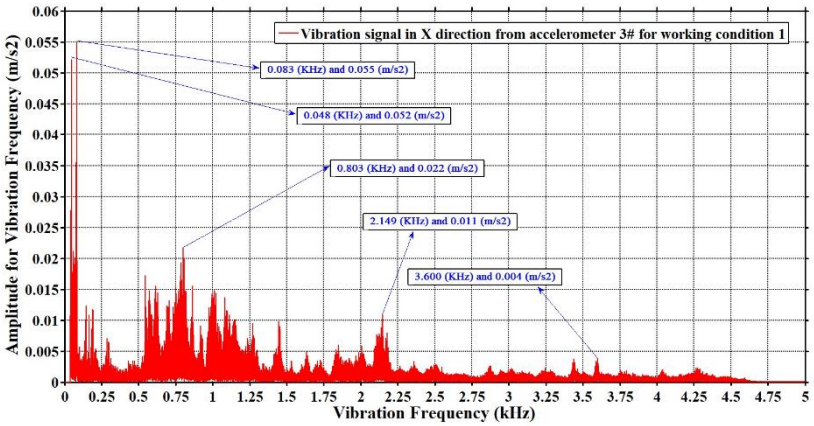
Vibration signal in X direction from accelerometer 3# for working condition 1
0.083 (KHz) and 0.055 (m/s2)
0.048 (KHz) and 0.052 (m/s2)
0.803 (KHz) and 0.022 (m/s2)
2.149 (KHz) and 0.011 (m/s2)
3.600 (KHz) and 0.004 (m/s2)
Amplitude for Vibration Frequency (m/s2)
Vibration Frequency (kHz)

(d)

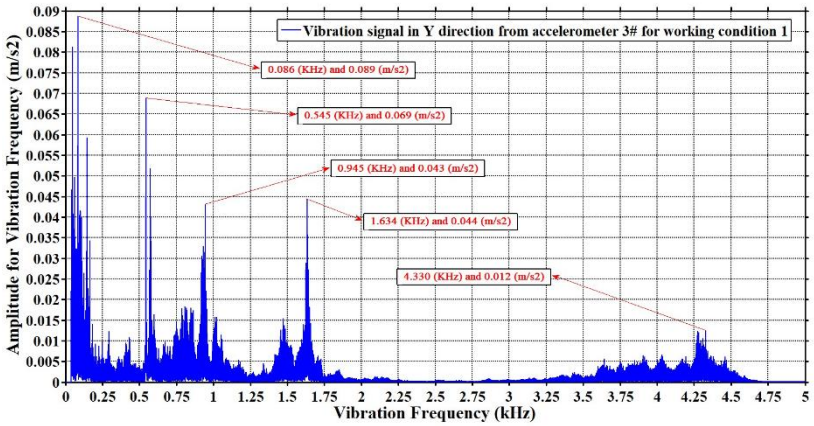
Vibration signal in Y direction from accelerometer 3# for working condition 1
0.086 (KHz) and 0.089 (m/s2)
0.545 (KHz) and 0.069 (m/s2)
0.945 (KHz) and 0.043 (m/s2)
1.634 (KHz) and 0.044 (m/s2)
4.330 (KHz) and 0.012 (m/s2)
Amplitude for Vibration Frequency (m/s2)
Vibration Frequency (kHz)

(e)

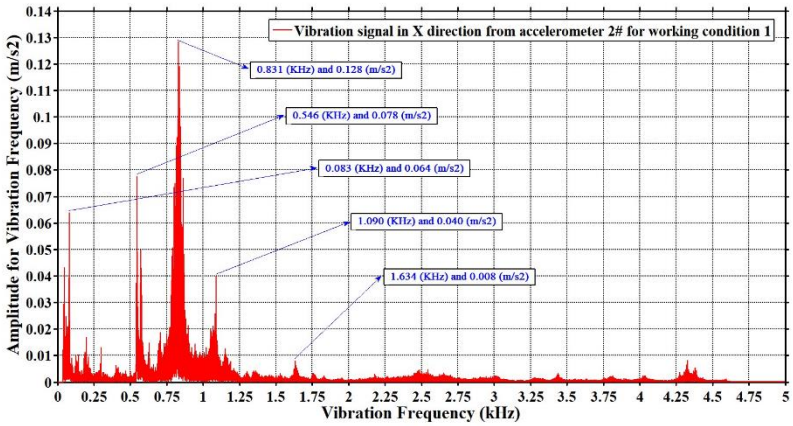
Vibration signal in X direction from accelerometer 2# for working condition 1
0.831 (KHz) and 0.128 (m/s2)
0.546 (KHz) and 0.078 (m/s2)
0.083 (KHz) and 0.064 (m/s2)
1.090 (KHz) and 0.040 (m/s2)
1.634 (KHz) and 0.008 (m/s2)
Amplitude for Vibration Frequency (m/s2)
Vibration Frequency (kHz)

(f)

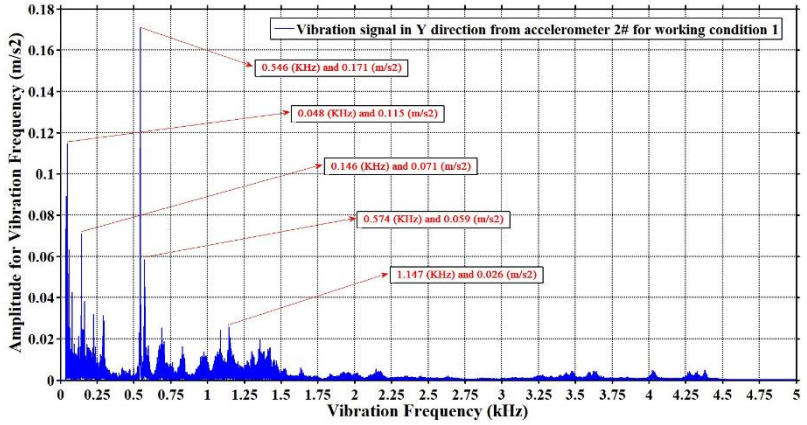

(g)

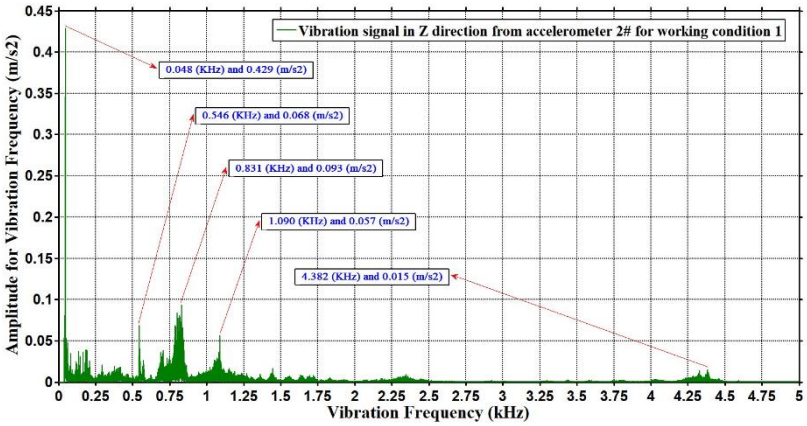

(h)

Fig. 8. Frequency-domain component features of vibration acceleration at different positions of the tower for Condition 1: (a) - (c): Acceleration components measured by Sensor 1# at the bottom of the tower; (d) - (e): Acceleration components measured by Sensor 3# in the middle of the tower; (f)-(h): Acceleration components measured by Sensor 2# at the top of the tower.

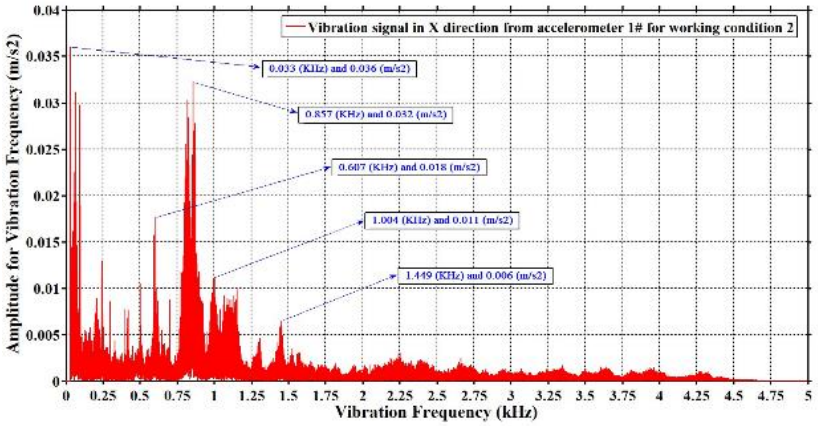

(a)

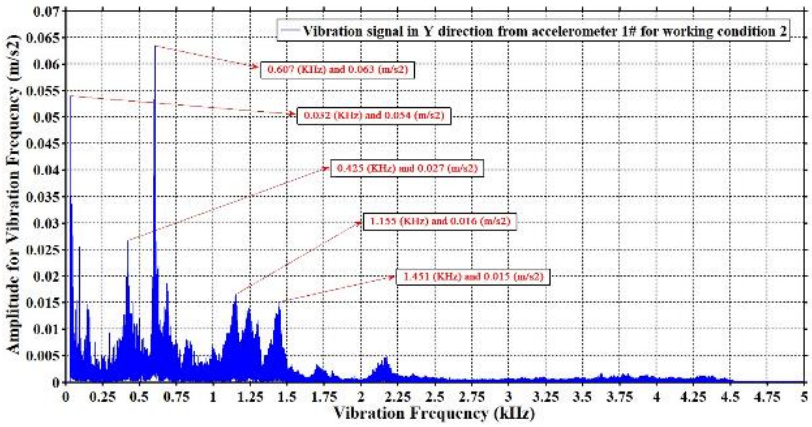
Vibration signal in Y direction from accelerometer 1# for working condition 2
0.607 (KHz) and 0.063 (m/s2)
0.032 (KHz) and 0.054 (m/s2)
0.425 (KHz) and 0.027 (m/s2)
1.155 (KHz) and 0.016 (m/s2)
1.451 (KHz) and 0.015 (m/s2)
Amplitude for Vibration Frequency (m/s2)
Vibration Frequency (kHz)

(b)

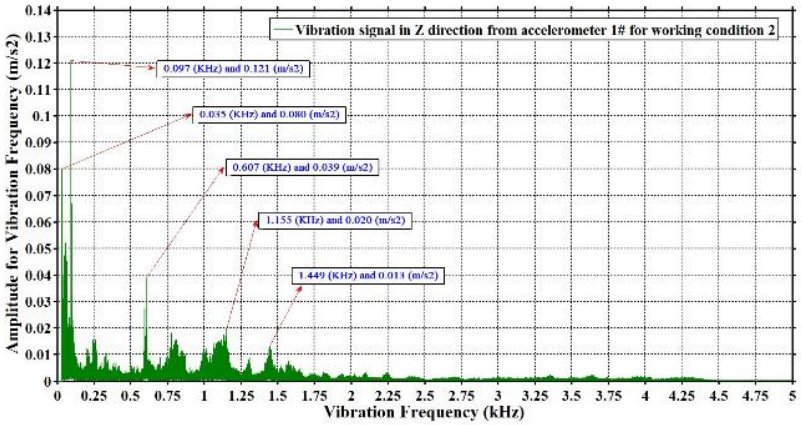
Vibration signal in Z direction from accelerometer 1# for working condition 2
0.097 (KHz) and 0.121 (m/s2)
0.035 (KHz) and 0.080 (m/s2)
0.607 (KHz) and 0.039 (m/s2)
1.155 (KHz) and 0.020 (m/s2)
1.449 (KHz) and 0.013 (m/s2)
Amplitude for Vibration Frequency (m/s2)
Vibration Frequency (kHz)

(c)

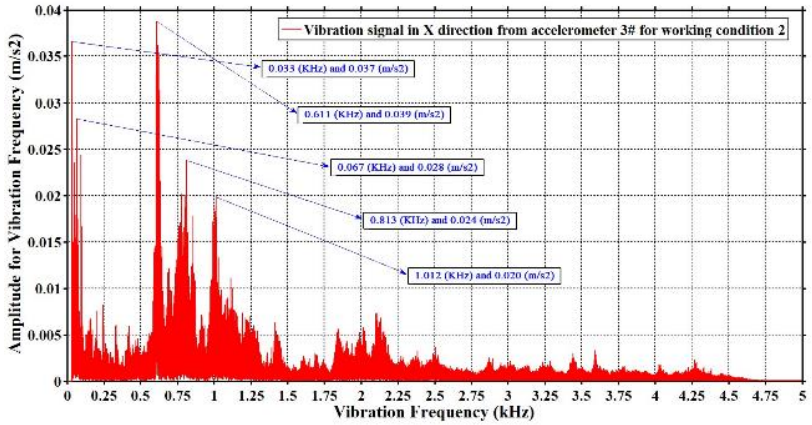
Vibration signal in X direction from accelerometer 3# for working condition 2
0.033 (KHz) and 0.037 (m/s2)
0.611 (KHz) and 0.039 (m/s2)
0.067 (KHz) and 0.028 (m/s2)
0.813 (KHz) and 0.024 (m/s2)
1.012 (KHz) and 0.020 (m/s2)
Amplitude for Vibration Frequency (m/s2)
Vibration Frequency (kHz)

(d)

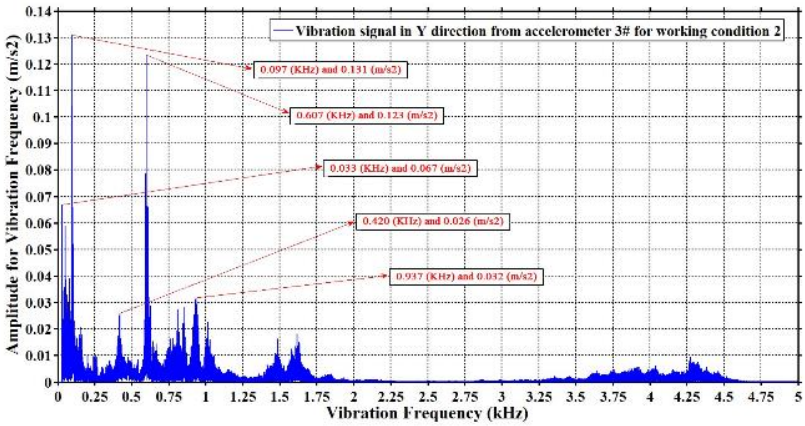
Vibration signal in Y direction from accelerometer 3# for working condition 2
0.097 (KHz) and 0.131 (m/s2)
0.607 (KHz) and 0.123 (m/s2)
0.033 (KHz) and 0.067 (m/s2)
0.420 (KHz) and 0.026 (m/s2)
0.937 (KHz) and 0.032 (m/s2)
Amplitude for Vibration Frequency (m/s2)
Vibration Frequency (kHz)

(e)

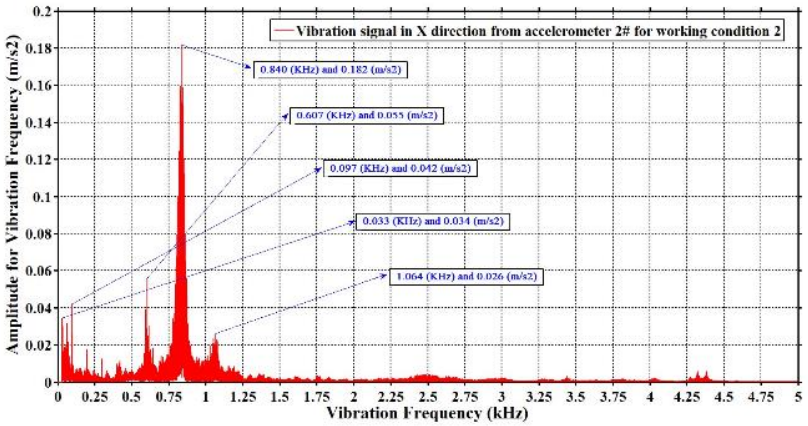

(f)

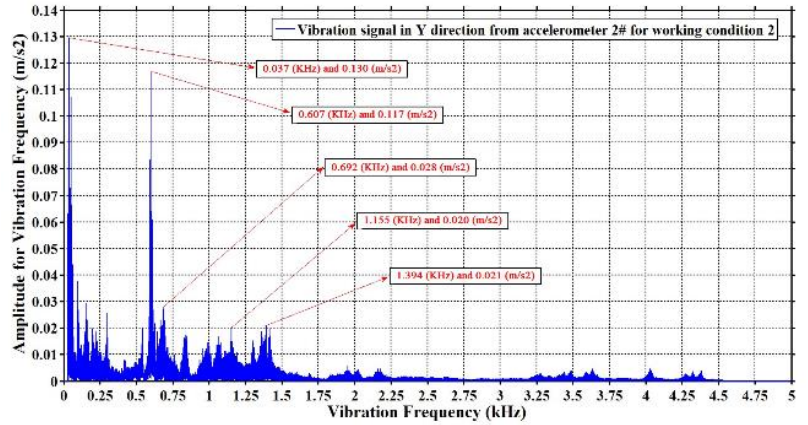

(g)

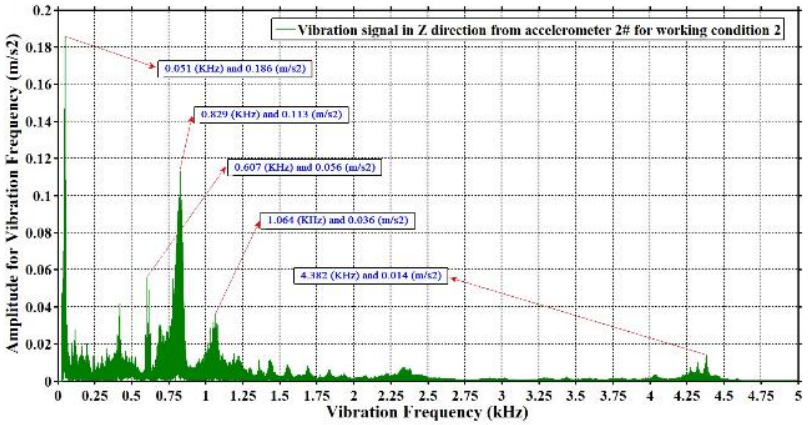

(h)

Fig. 9. Frequency-domain component features of vibration acceleration at different positions of the tower for condition 2: (a) -(c): Acceleration components measured by Sensor 1# at the bottom of the tower; (d) - (e): Acceleration components measured by Sensor 3# in the middle of the tower; (f) - (h): Acceleration components measured by Sensor 2# at the top of the tower.

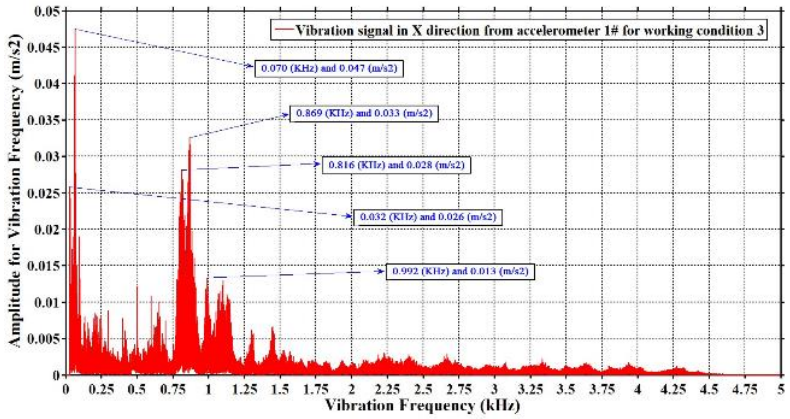
Vibration signal in X direction from accelerometer 1# for working condition 3
0.070 (KHz) and 0.047 (m/s2)
0.869 (KHz) and 0.033 (m/s2)
0.816 (KHz) and 0.028 (m/s2)
0.032 (KHz) and 0.026 (m/s2)
0.992 (KHz) and 0.013 (m/s2)
Amplitude for Vibration Frequency (m/s2)
Vibration Frequency (kHz)

(a)

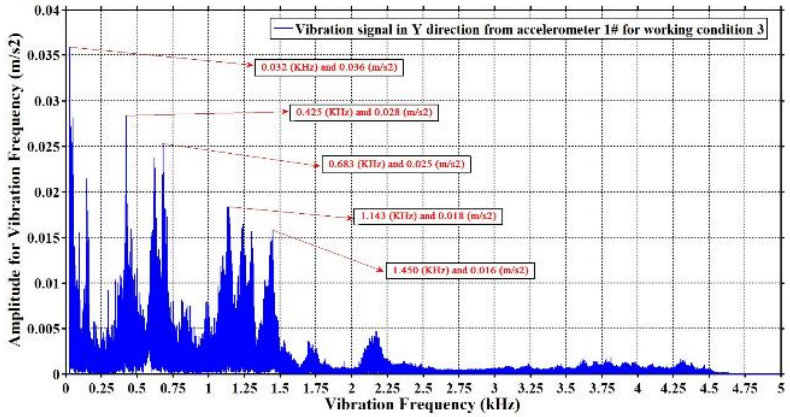
Vibration signal in Y direction from accelerometer 1# for working condition 3
0.032 (KHz) and 0.036 (m/s2)
0.425 (KHz) and 0.028 (m/s2)
0.683 (KHz) and 0.025 (m/s2)
1.143 (KHz) and 0.018 (m/s2)
1.450 (KHz) and 0.016 (m/s2)
Amplitude for Vibration Frequency (m/s2)
Vibration Frequency (kHz)

(b)

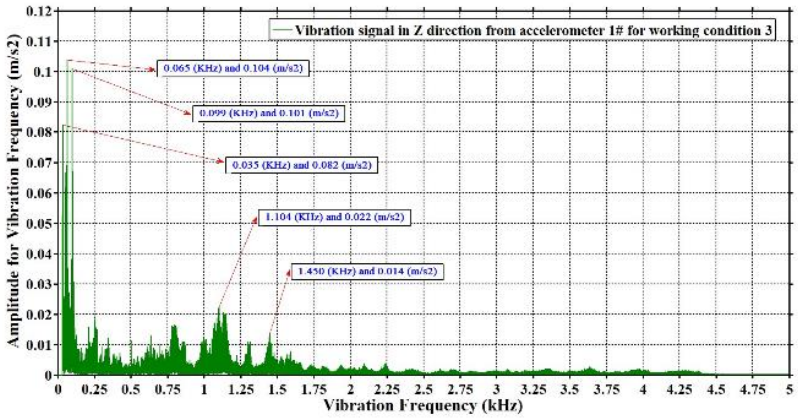
Vibration signal in Z direction from accelerometer 1# for working condition 3
0.065 (KHz) and 0.104 (m/s2)
0.099 (KHz) and 0.101 (m/s2)
0.035 (KHz) and 0.082 (m/s2)
1.104 (KHz) and 0.022 (m/s2)
1.450 (KHz) and 0.014 (m/s2)
Amplitude for Vibration Frequency (m/s2)
Vibration Frequency (kHz)

(c)

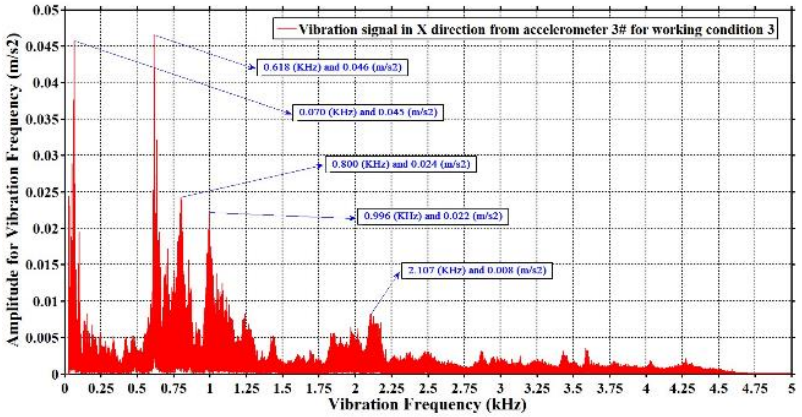
Vibration signal in X direction from accelerometer 3# for working condition 3
0.618 (KHz) and 0.046 (m/s2)
0.070 (KHz) and 0.045 (m/s2)
0.800 (KHz) and 0.024 (m/s2)
0.996 (KHz) and 0.022 (m/s2)
2.107 (KHz) and 0.008 (m/s2)
Amplitude for Vibration Frequency (m/s2)
Vibration Frequency (kHz)

(d)

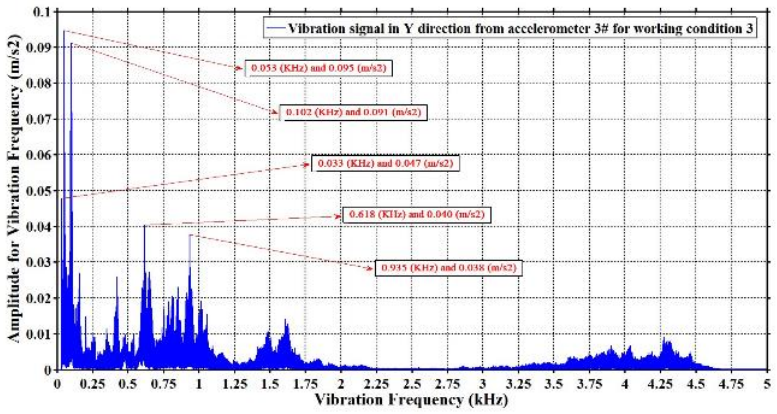

(e)

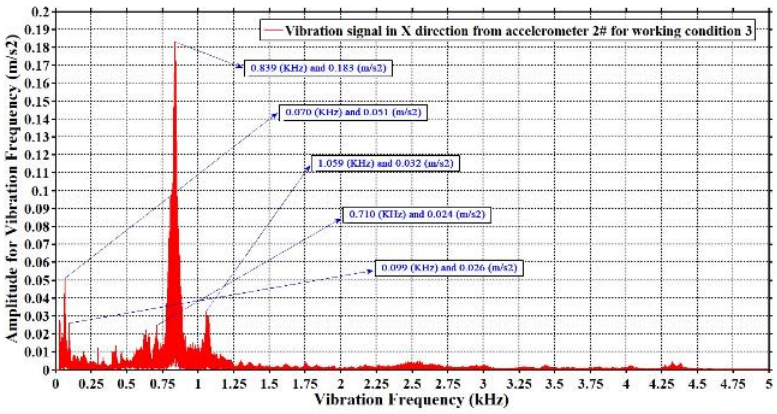

(f)

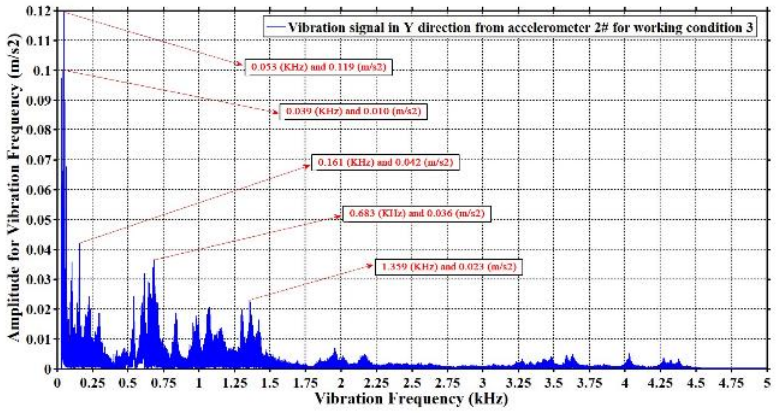

(g)

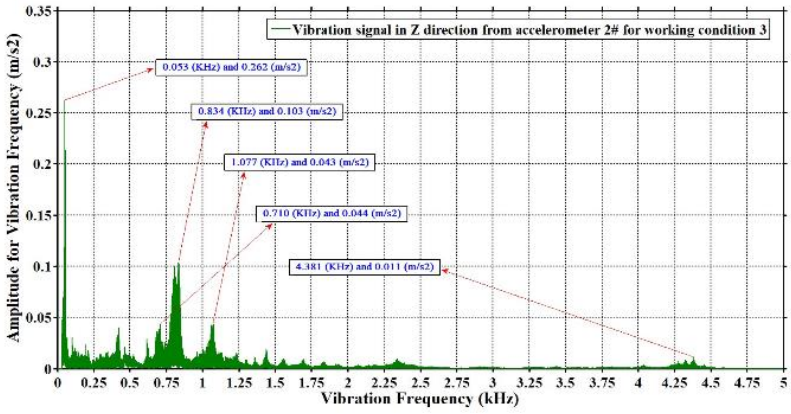

(h)

Fig. 10. Frequency-domain component features of vibration acceleration at different positions of the tower for Condition 3: (a) -(c): Acceleration components measured by Sensor 1# at the bottom of the tower; (d) - (e): Acceleration components measured by Sensor 3# in the middle of the tower; (f) - (h): Acceleration components measured by Sensor 2# at the top of the tower.

In Figures 8 to 10, according to the frequency components of vibration acceleration at different heights of the tower, 0 - 2 kHz is defined as the low-frequency part; 2 - 4 kHz is the intermediate frequency part, and 4 - 5 kHz is the high-frequency part. It can be seen that under the three working conditions (v = 12, 14, 16 *m/s*), from the bottom to the middle, and then to the top of the tower, the amplitudes of the vibration acceleration components at different heights of the 300W small wind turbine tower are located in the low-frequency part (f_{re} < 2 kHz). The peak of each amplitude (max in the figure) also occurs in the low frequency stage. The amplitude of the vibration acceleration component in all directions of the middle and high frequency part (f_{re} > 2 kHz) is small, implying that the main vibration pattern of the tower is low-frequency vibration.

It is also observed that under the three working conditions, the y direction of Sensor3# in the middle of the tower and the z direction of Sensor 2# at the top of the tower ((e) and (h) in Figures 8-10) have high-frequency vibration components in the middle and high frequency of the frequency domain (f >2kHz). Their frequencies are in the ranges of about 3-4.75 kHz and 4-4.5 kHz, respectively. This indicates that the lateral vibration in the tower and the axial vibration characteristics at the top of the tower cannot be ignored. For the high-frequency vibration in the z-direction of Sensor 2# at the top of the tower, it is because the axial wind-induced vibration caused by the aerodynamic load in the z-direction dominates the vibration pattern. For the y direction high-frequency vibration of Sensor 3#, it is because fixed constraints are applied at the bottom of the tower due to its special position. The axial wind induced vibration at the top of the tower is mainly caused by the aerodynamic load in the z-direction. Hence, the lateral vibration caused by yawing oscillation can only be reflected in the middle of the tower.

The peaks of the isotropic vibration acceleration component at different heights of the tower are compared, as shown in Table 3.

Table 3. Frequency component peak of vibration acceleration at different locations.

Locations		Condition 1	Condition 2	Condition 3
1# (Bottom)	*x*	0.067	0.036	0.047
	y	0.088	0.063	0.036
	z	0.132	0.121	0.104
3# (Middle)	*x*	0.055	0.039	0.046
	y	0.089	0.130	0.095
2# (Top)	*x*	0.128	0.182	0.183
	y	0.171	0.130	0.119
	z	0.429	0.186	0.262

Comparing the vibration acceleration components under the three working conditions in Table 3, it is found that the peaks of the vibration acceleration components in the x, y and z directions at the top of the tower (**2#**) reach the maximum values, with 0.183, 0.119 and 0.262 m/s^2, respectively. They are significantly greater than the peaks in the middle (3#) and at the bottom (1#) of the tower under the other two working conditions. It indicates that the vibration at the top of the tower is the most severe compared with the bottom and the middle of the tower.

Comparing the vibration acceleration signals in the same direction, it is found that under the three working conditions, from the bottom to the middle and then to the top of the tower, there are obvious amplitudes of vibration acceleration in the x direction around f_{re} = 0.8 kHz (shown as (a), (d), and (f) in Figures 8 to 10); that in the y direction around f_{re} = 0.6 kHz (shown as (b), (e), and (g)); that in the z direction around f_{re} = 0.1, 0.8, and1.0 kHz (shown as (c), and (h)). The reason is that these frequency peaks are close to the natural frequency components of the tower in the three directions.

5. CONCLUSION

The vibration characteristics of the tower of a 300W horizontal axis wind turbine are investigated through the vehicle test. Time-frequency of the vibration acceleration component at different heights of the tower under different wind conditions is analyzed, and the following conclusions are obtained:

1) The main vibration pattern of the tower is low-frequency vibration.
2) Under natural wind loading, the vibration response at the top of the tower is the most significant, and its vibration is mainly caused by the aerodynamic load.
3) The lateral vibration in the middle of the tower and the axial vibration characteristics at the top of the tower are obvious, which are the main motivating factors affecting the vibration of the tower structure.
4) As the tower height and wind speed increase, the vibration response of the vehicle wind turbine system (z-direction) is the most obvious, while the vertical and lateral (x and y) vibration responses are all related to wind speed and height.

5) When the test wind speed is the maximum, the peaks of the vibration acceleration components in the three directions at the top of the tower reach the maximum, with 0.183, 0.119 and 0.262 m/s^2, respectively. Both are significantly larger than the peaks in the middle and at the bottom of the tower under the other two low test wind speeds. It further shows that compared with the bottom and the middle of the tower, the vibration at the top of the tower is the most severe.
6) The vibration characteristics of the wind turbine tower are tested by the vehicle test method, and an optimal test effect is achieved. The feasibility of the vehicle test of the wind turbine is verified. It lays a foundation for the vibration test of horizontal axis wind turbine in the future and provides an effective reference for ensuring the safety and reliability design of the tower, and the low-frequency vibration status monitoring of wind turbines.
7) Because the vibration test equipment used in this test has good environmental applicability, the influence of environmental factors (such as temperature, humidity, etc.) on the measurement results can be ignored.

ACKNOWLEDGEMENT

This research was funded by the Chongqing Natural Science Foundation of China (No. cstc2020jcyj-msxmX0314), the Ningxia key Research and Development Program of Foreign Science and Technology Cooperation Projects (No. 202204), the Key Scientific Research Project in Higher Education Institutions from Ningxia Education Department (No. 2022115), and the PhD Start-up Fund from Chongqing University of Science and Technology (No. 181903017).

REFERENCES

[1] Li Y., Lan Y., Li Q., Lei Z., and Liu G., 2020. Research and method summary on vibration control of wind turbine tower structure. *Ship Engineering* 42(S2): 248-253. DOI: 10.13788/j.cnki.cbgc.2020.S2.048.
[2] Su L., Zhu J., Guo G., and Li Y., 2023. Research on wind turbine tower vibration monitoring based on XGBoost and Wasserstein distance. *Acta Energiae Solaris Sinica* 44(01): 306-312. DOI: 10.19912/j.0254-0096.tynxb.2021-0924.
[3] Wang X., 2022. Seismic dynamic response and stability study of wind turbine tower, Changzhou University. DOI: 10.27739/d.cnki.gjsgy.2022.000457.
[4] Lei Z., Liu G., Wang H., and Liu Q., 2022. Investigation on vibration control performance of wind turbine tower using a prestressed tuned mass damper under seismic excitations. *China Civil Engineering Journal* 55(S1): 92-100. DOI: 10.15951/j.tmgcxb.2022.s1.0410.
[5] Xiang S., 2020. Research on vibration control technology for flexible towers of offshore wind turbines. Shenyang University of Technology. DOI: 10.27322/d.cnki.gsgyu.2020.000059.
[6] Yang W., Chai Y., Zheng J., and Liu J., 2022. Vibration frequency tracking of wind turbine tower using parallel adaptive notch filter. *Acta Energiae Solaris Sinica* 43(08): 309-315. DOI: 10.19912/j.0254-0096.tynxb.2020-1341.
[7] Gu C., Chen D., Liu F., Fang K., Guo D., and Marzocca P., 2021. Dynamic analysis of flexible wind turbine tower by a transfer matrix method. *International Journal of Structural Stability and Dynamics* 21(10): 2150142. https://doi.org/10.1142/S021945542150142X.
[8] Xiao Z., 2022. Analysis of mechanical properties of horizontal axis wind turbine tower structure and optimization design of wind resistance. Guangzhou University. DOI: 10.27040/d.cnki.ggzdu.2022.000314.
[9] Li Z., Dong B., Ma J., and Li G., 2022. Comparison between the modal parameters of the wind turbine tower-blade coupling structure and those of a single blade. *Journal of Xi'an Technological University* 42(06): 565-572. DOI: 10.16185/j.jxatu.edu.cn.2022.06.202.
[10] Guan C. and C.L. Tian, 2021. Modal analysis method and comparison for wind turbine tower. *Acta Energiae Solaris Sinica* 42(04): 473-478. DOI: 10.19912/j.0254-0096.tynxb.2018-1383.
[11] Deng M., Deng A., Zhu J., Xu Q., Wang S., and Wang S., 2021. Research on real-time state of wind turbine tower based on modal superposition method. *Acta Energiae Solaris Sinica* 42(03): 63-70. DOI: 10.19912/j.0254-0096.tynxb.2018-1091.
[12] Yu Q., Li X., Xu G., Ren J., Zhuo P., and Sun Y., 2019. Testing and analysis of the natural frequency of wind turbine tower based on strain mode. *Solar Energy* (10): 66-69.
[13] Chen T., Wang Q., Du K., Wang C., and Zhang L., 2016. Application of modal analysis in low frequency vibration of wind turbine tower. *2016 Annual Meeting of the Chinese Society of Electrical Engineering* 1-5.
[14] Malliotakis G., Alevras P., and Baniotopoulos C., 2022. Recent advances in vibration control methods for wind turbine towers. *Energies* 14(22): 7536. https://doi.org/10.3390/en14227536.
[15] Diken H and S. Asiri. 2023. Vibration analysis of horizontal axis wind turbine considering tower-nacelle-foundation interaction. *Journal of Vibration Engineering and Technologies*. DOI:10.1007/s42417-023-00946-0.
[16] Pollini N., Pegalajar-Jurado A., and Bredmose H., 2023. Design optimization of a tetra spar-type floater and tower for the IEA wind 15 MW reference wind turbine. *Marine Structures* 90: 103437. https://doi.org/10.1016/j.marstruc.2023.103437.
[17] Yan S., Wang J., and Zhang J., 2023. Analysis of stress characteristics of wind turbine tower considering dynamic change of wind direction. *Acta Energiae Solaris Sinica* 44(04): 140-146. DOI: 10.19912/j.0254-0096.tynxb.2021-1539.

[18] Wu Y., Gao Z., Wang J., Chen Y., Li X., Liu K., and Chen T., 2021. Experimental study on frequency and mode characteristics of horizontal axis wind turbine tower. *Renewable Energy Resources* 39(01): 50-55. DOI: 10.13941/j.cnki.21-1469/tk.2021.01.009.

[19] Chen T., Gao Z., Jiang X., Hou Y., and Wang J., 2018. Based on sensor for the axial and transverse vibration characteristics analysis of wind turbine tower. *Instrument Technique and Sensor* (8): 76-80.